Interplay between interstitial displacement and displacive lattice transformations

Xie Zhang,[1,*] Tilmann Hickel,[1] Jutta Rogal,[2] and Jörg Neugebauer[1]
[1]*Max-Planck-Institut für Eisenforschung GmbH, 40237 Düsseldorf, Germany*
[2]*Interdisciplinary Centre for Advanced Materials Simulation, Ruhr-Universität Bochum, 44780 Bochum, Germany*
(Received 7 April 2016; revised manuscript received 6 July 2016; published 12 September 2016)

Diffusionless displacive lattice rearrangements, which include martensitic transformations, are in real materials often accompanied by a displacive drag of interstitials. The interplay of both processes leads to a particular atomistic arrangement of the interstitials in the product phase, which is decisive for its performance. An archetype example is the martensitic transformation in Fe-C alloys. One of the puzzles for this system is that the deviation from the cubic symmetry (i.e., the tetragonality) in the martensite resulting from this interplay is lower than what thermodynamics dictates. In our *ab initio* approach, the relative motion of C in the transforming lattice is studied with the nudged elastic band method. We prove that an atomic shearlike shuffle mechanism of adjacent $(11\bar{2})$ Fe layers along the $\pm[111]_{bcc}$ directions is essential to achieve a redistribution of C atoms during the fcc $\rightarrow$ bcc transition, which fully explains the abnormal behavior. Furthermore, the good agreement with experiment validates our method to treat a diffusionless redistribution of interstitials and a displacive rearrangement of the host lattice simultaneously.

DOI: 10.1103/PhysRevB.94.104109

I. INTRODUCTION

Martensitic transformations are diffusionless solid-solid transformations where atoms move collectively and require only small (on the scale of atomic bond lengths) displacements. These transformations are often temperature driven, with the high-temperature phase having a higher symmetry than the low-temperature one (see, e.g., Ref. [1]). When changing the symmetry of the underlying lattice, a material with identical chemical composition will exhibit a significant change in its properties, an effect which is heavily employed in many applications. For example, martensitic transformations are at the heart of shape memory alloys [2,3], magnetocaloric materials [4,5], or are used to increase the strength in steels [6].

In addition to such displacive rearrangements of the host lattice, a transport of interstitial atoms from the parent to the product lattice is often involved. In these cases, there exists a sophisticated interplay of the two concurrent subprocesses. On the one hand, depending on their distinct chemical and elastic properties, the interstitial atoms may hinder or promote the rearrangement of the host lattice (see, e.g., Ref. [7]). On the other hand, specific transformation paths of the host lattice give rise to different occupations of the interstitials in the product lattice. Understanding the atomic-scale interplay of the two subprocesses is a prerequisite to tune the stability and mechanical properties of the product phase since the latter is strongly affected by the distribution of interstitial atoms.

The prototype example is the martensitic transformation of Fe-C alloys, which are thermodynamically stable at high temperatures in the face-centered-cubic (fcc) phase named austenite and transform at low temperatures into a tetragonally distorted body-centered-cubic (bcc) phase called martensite. During the transformation, C interstitials are redistributed onto three octahedral sublattices in martensite. Despite the fact that martensitic transformations were first discovered in steels and have been extensively investigated, the experimentally observed abnormally low tetragonality due to an interplay between the redistribution of C interstitials and the fcc $\rightarrow$ bcc Fe transformation has not been well understood so far.

As we will discuss in detail in Sec. II, the established picture for the martensitic transformation in steels has been challenged since the mid-1960s by a series of experiments finding an abnormally low or high tetragonality of the martensite. Even though there have been a number of mechanisms proposed to explain the abnormal behavior, to date a convincing picture is still missing. Hence, the Fe-C system is well suited to understand the atomistic interplay between interstitial redistribution and a displacive transformation of the host lattice since the tetragonality observed in abundant experiments allows us to quantitatively validate the atomistic mechanisms we identify.

In this work, we employ an *ab initio* nudged elastic band (NEB) approach to calculate the minimum-energy paths (MEPs) of the martensitic transformation in Fe-C alloys based on our recently discovered lattice correspondence between austenite and martensite [8]. These simulations reveal that the abnormally low tetragonality of the martensite results from a drag effect of C interstitials by the shearlike shuffle of adjacent $(11\bar{2})$ Fe layers along the $\pm[111]_{bcc}$ directions during the displacive transformation. The major distinction of the current transformation path is that it shows, next to a shear component, also an atomic shuffle, which was absent in the previously suggested ones and which is shown to be the origin of the abnormal occupation.

This paper is organized as follows: We first briefly review the experiments that challenge the conventional picture for the martensitic transformation in Fe-C alloys, and discuss the existing explanations in Sec. II. Then we discuss how to construct a lattice correspondence for the diffusionless redistribution of C interstitials onto the three octahedral sublattices in martensite in Sec. III. The computational details are described in Sec. IV. Furthermore, the MEPs of the structural transformation from austenite to martensite are calculated and analyzed for different C redistribution scenarios in Sec. V. Afterwards, the mechanism of the martensite formation is

*Corresponding author: x.zhang@mpie.de

systematically discussed in Sec. VI in order to reveal the fundamental distinction of the current transformation path from the previous ones. Finally, the major conclusions of this work are summarized in Sec. VII.

II. TRANSFORMATION PATHS IN FE-C ALLOYS

It was found in 1926 and 1927 [9,10] that martensite has a body-centered-tetragonal (bct) crystal structure. Two years later, Kurdjumov and Kaminsky [11,12] experimentally observed a linear relation between the two lattice parameters of martensite, c and a, and the C concentration. Based on these studies, the Fe-C martensite could be identified as a supersaturated solid solution of C in which C interstitials occupy only one out of the three octahedral sublattices in bcc Fe.

The occupation of only one of the three sublattices was explained in terms of a Bain [13] transformation path, which describes a continuous deformation from fcc to bcc. As shown in Fig. 1(a), a bct cell (marked and shaded blue) can be derived from fcc austenite. The octahedral interstitial sites (OISs) inherited from fcc austenite transform to only one out of the three possible octahedral sublattices in the bcc phase. Occupying only one of the sublattices destroys the cubic symmetry and results in the tetragonally distorted bct structure. This also holds for transformation paths based on the commonly observed orientation relationships (ORs) between austenite and martensite, namely, Kurdjumov-Sachs (KS) [14] and Nishiyama-Wassermann (NW) [15,16] ORs. As shown in Fig. 1(b), with a homogenous deformation mechanism (no atomic shuffle involved), these paths would transfer all C interstitials in austenite onto a single octahedral sublattice (colored green) in martensite.

The above understanding of the Fe-C martensite is intuitive and widely accepted. However, experiments starting in the mid-1960s challenged this picture. These experiments revealed an abnormally low tetragonality in the freshly formed martensite in Mn, low-Ni, Rh, and Cr steels [17–20]. This results from a considerable amount of the C interstitials occupying the other two sublattices. Quantitative analyses based on neutron diffractions of a steel sample (8 wt.% Ni and 1.5 wt.% C) showed that only ∼80% of C atoms occupy the same octahedral sublattice [21]. Even though there might also be some C atoms segregated to grain boundaries or dislocations, the large deviation of the tetragonality from its ideal value

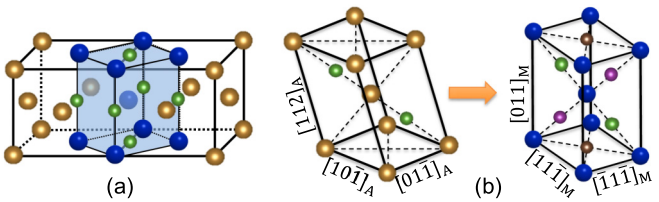

FIG. 1. Schematic representation of transformation paths based on the (a) Bain [13] and (b) Kurdjumov-Sachs [14] or Nishiyama-Wassermann [15,16] orientation relationships between fcc and bcc Fe. The large colored spheres represent Fe atoms, while the small spheres (green, brown, and purple) denote C atoms on three different octahedral sublattices, respectively.

demonstrates the existence of a remarkable partial disordering of C interstitials on the octahedral sublattices. In particular, atom probe tomography reveals that the C distribution in the freshly formed martensite (or virgin martensite) is purely homogenous [22]. In contrast, the freshly formed martensite in Al and high-Ni steels exhibits an abnormally high tetragonality (the concentration dependence is ∼1.5 times higher than the normal case) [23,24], whereas in Fe-Mn-C alloys, it is orthorhombic rather than tetragonal [25]. These experimental observations could not be explained by the conventionally well-established transformation paths.

To address the incomplete ordering, various mechanisms have been proposed. Specifically, Lyssak and Nikolin [26] suggested that the austenite → martensite transition in Mn and Re steels occurs through an intermediate hexagonal ϵ martensite, which leads to a redistribution of half of the C atoms into OISs and the other half into tetrahedral interstitial sites (TISs). This mechanism was, however, questioned by neutron-diffraction experiments [21] showing that C atoms do not occupy the TISs in martensite.

An alternative mechanism was proposed by Roitbourd and Khachaturyan [27], and later carefully interpreted by Kurdjumov [28–30]. They proposed that the martensitic transformation is accompanied by the formation of $[01\bar{1}](011)_M$ twins corresponding to the $[11\bar{2}](111)_A$ twins, where the subscripts "M" and "A" stand for martensite and austenite, respectively. The formation of such twins allows C redistribution onto another sublattice. However, as pointed out by Kajiwara and Kikuchi [31], and Christian [32], there is no direct evidence for the existence of such small twins, though large-scale $(01\bar{1})$ twins have been reported before [33].

Other concepts invoked [31,34–37] the morphology of the martensite, strong dipole configurations, the formation of an $L1_2$ superlattice, or substitutional alloy elements to explain the anomalies in the tetragonality.

All currently available interpretations can be summarized into two categories: (i) The abnormally low tetragonality is attributed to part of the C atoms occupying the other two octahedral sublattices; (ii) the abnormally high tetragonality is related to substitutional alloy elements, the formation of superstructures, or the morphology, etc.

Here, the focus is on the abnormally low tetragonality for which the previous discussion indicates that a proper description of the atomistic transformation path in Fe-C alloys is crucial. Since the conventional paths as discussed above lead to a perfect ordering, we use our recently proposed transformation path [8] that connects austenite, ferrite, and cementite (Fe_3C) in a unified framework. In that approach, a displacive rearrangement of Fe lattices and a diffusional redistribution of C interstitials were combined. In this study, we will extend this approach to the case of fully diffusionless martensitic transformation in Fe-C alloys. The details of how we construct the lattice correspondence will be described in the next section.

III. LATTICE CORRESPONDENCE

To calculate the MEP of the austenite → martensite transformation in the Fe-C system, a key issue is the determination of the lattice correspondence between austenite and

martensite. In our recently established lattice correspondence [8], a metastable intermediate structure (MIS) that serves as a central link for the structural transformations among austenite, ferrite, and cementite was identified. The MIS itself originates from a structural relaxation of cementite after excluding all C atoms in the ferromagnetic (FM) state. It consists of a periodic arrangement of $\Sigma 3$ twin boundaries in bcc Fe and is an interface structure similar to the concept of complexions [38], which undergoes structural transformations to austenite, ferrite, and cementite depending on the local conditions. Using this lattice correspondence, we constructed a unified transformation path that combines the displacive rearrangement of Fe lattices and the diffusional redistribution of C interstitials. We will show in the following that even if there is no formation of cementite, the transformation path involving the MIS is essential for the formation of martensite.

In the present study, we therefore extend this approach to the case of martensitic transformations where the C redistribution is also diffusionless. Based on this approach, orthorhombic cells for austenite, the MIS, and martensite including all available OISs can be derived, as shown in Fig. 2. Combining the atomic positions in both austenite and martensite within a single orthorhombic cell [Fig. 2(c)], one can clearly see that there exists a natural correspondence between the atomic positions of Fe atoms in austenite and martensite with the MIS in between. Figure 3 also shows that any of the available OISs in austenite (colored red) has a closer correspondence to a particular octahedral sublattice, sublattice 1 (colored green), than to the other two sublattices in martensite. Specifically, as shown in Fig. 3(a), a three-dimensional comparison between the structures of austenite and martensite intuitively reveals

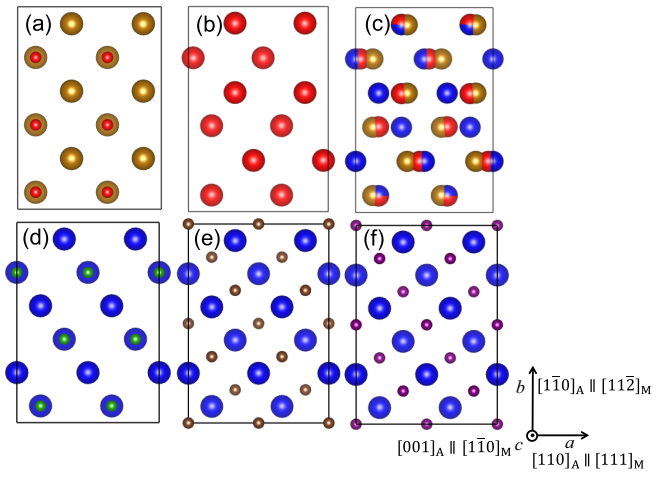

FIG. 2. (a) Unit cell of austenite with all available octahedral interstitial sites. (b) Unit cell of the MIS. (c) A comparison of the atomic positions of Fe atoms in austenite (gold), the MIS (red), and martensite (blue). (d)–(f) The unit cell of martensite with three octahedral sublattices, respectively. The lattice constants of the shown unit cells can be found in Table I. The small red spheres represent C in the octahedral interstitial sites in austenite. The other small colored spheres represent C on different sublattices of octahedral interstitial sites in martensite: green is sublattice 1; brown is sublattice 2; purple is sublattice 3. The structures in this paper are visualized using the VESTA program [39].

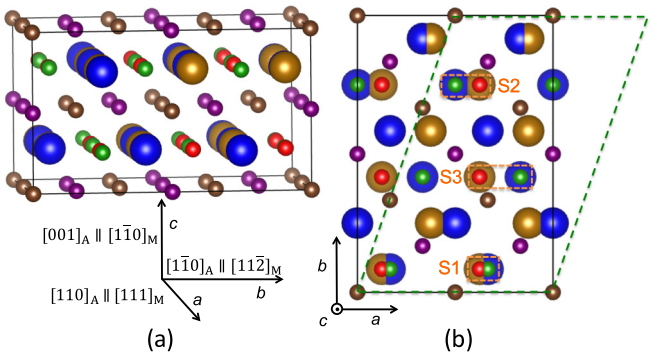

FIG. 3. Lattice correspondence between austenite and martensite with the same color code as in Fig. 2: (a) Three-dimensional structural visualization; (b) projection on the ab plane. In this lattice correspondence, austenite and martensite follow the Pitsch OR [40], i.e., $[110]_A||[111]_M$, $[1\bar{1}0]_A||[11\bar{2}]_M$, and $[001]_A||[1\bar{1}0]_M$, where subscripts "A" and "M" stand for austenite and martensite, respectively. The small orange boxes and letters in (b) label the three different scenarios for C redistribution. The large green dashed box in (b) shows another construction of the unit cell of martensite, which yields a different lattice correspondence between austenite and martensite.

that all OISs in austenite are located in the same atomic chains as the OISs of sublattice 1 in martensite.

However, as visualized in Fig. 3(b), the correspondence is not perfect. Among all OISs of sublattice 1, there are three kinds of scenarios, labeled in Fig. 3(b) by S1, S2, and S3. For scenarios S1 and S2, all OISs in austenite exhibit a natural correspondence to sublattice 1 crystallographically. However, it becomes indeterminate for scenario S3 since the distances between the OISs in austenite and the neighboring OISs of the three sublattices in martensite become comparable. We will show in the following that the different quality of the correspondence for the three sublattices provides an intuitive explanation for the experimentally observed incomplete ordering.

IV. COMPUTATIONAL DETAILS

To calculate the MEPs of the martensitic transformation in Fe-C alloys, we employ standard and generalized solid-state NEB (SSNEB) methods as implemented in the VTST code [41–43]. All NEB and SSNEB simulations are carried out with energies and forces obtained from spin-polarized density-functional-theory (DFT) calculations.

To describe the electron-ion interactions, we employ Blöchl's projector augmented wave (PAW) potentials [44] in combination with the Perdew-Burke-Ernzerhof (PBE) parametrization [45] of the exchange-correlation functional as implemented in the Vienna *Ab initio* Simulation Package (VASP) [46]. We perform systematic convergence tests on fcc and bcc Fe in the FM state. Our convergence checks show that the use of a plane-wave energy cutoff of $E_{\text{cut}} = 400$ eV, and $\sim$10 000 **k** points $\times$ atoms resulting from a homogeneous Monkhorst-Pack sampling [47] of the Brillouin zone can ensure an accurate description for both fcc and bcc Fe. A first-order Methfessel-Paxton scheme [48] with a thermal

TABLE I. Optimized lattice constants of the orthorhombic cells of austenite, martensite, and the MIS.

Structures	a (Å)	b (Å)	c (Å)
Austenite (without C, fcc)	5.148	7.722	3.640
Austenite (without C, fct)	4.841	7.264	4.016
Austenite (with one C atom)	4.978	7.490	3.951
Martensite (without C)	4.909	6.942	4.008
MIS (without C)	4.860	7.164	4.033

smearing parameter of 0.2 eV is used for integration over **k** points.

The optimized structural and magnetic properties of both fcc Fe (lattice constant 3.640 Å and magnetic moment 2.5 μ_B/atom) and bcc Fe (lattice constant 2.834 Å and magnetic moment 2.2 μ_B/atom) are in good agreement with previous experimental data [49] and theoretical results [50,51]. The corresponding lattice constants of the orthorhombic cells of austenite, martensite, and the MIS are listed in Table I. For the NEB simulations with C interstitials, the fully relaxed orthorhombic cell of FM austenite containing a single interstitial C atom is chosen as the reference of the simulation cell (see Table I). We note that using the martensite as a reference cell is not possible: Adding a single C atom would result in a tetrahedral distortion, rendering the three sublattice sites energetically as well as structurally inequivalent.

To describe the paramagnetic (PM) state of austenite and the MIS, we use the special quasirandom structures (SQS) approach as realized in the ATAT package [52]. The SQS method mimics the random distribution of magnetic moments of a PM state within a given supercell by approaching their correlation functions for the most relevant near-neighbor sites, pairs, triplets, etc. Collinear spin-up (50%) and spin-down (50%) magnetic moments (initially, 2.4 μ_B/atom) are distributed within a $1.5 \times 1 \times 2$ supercell (36 Fe atoms) relative to the orthorhombic unit cells as shown in Figs. 2 and 3 using a binary SQS. Notably, here we have a multiple of 1.5 since the orthorhombic cells shown are twice the primitive ones in the a direction.

V. STRUCTURAL TRANSFORMATIONS

In Sec. III, we constructed the lattice correspondence between austenite and martensite including all possible interstitial sites. While this gives some initial qualitative insight, to quantitatively understand the redistribution behavior of C interstitials during the austenite → martensite transition, it is essential to compute actual transformation paths in different scenarios. A key feature of our recently proposed path [8] of the fcc → bcc Fe transition is the occurrence of a MIS as an interface structure. Hence, in this section we will first revisit the austenite → MIS transition and then use this insight to derive the different scenarios for the C redistribution during the MIS → martensite transition. All of the structural details (animations and original structure files, etc.) of the following transformation pathways are provided in the Supplemental Material [53].

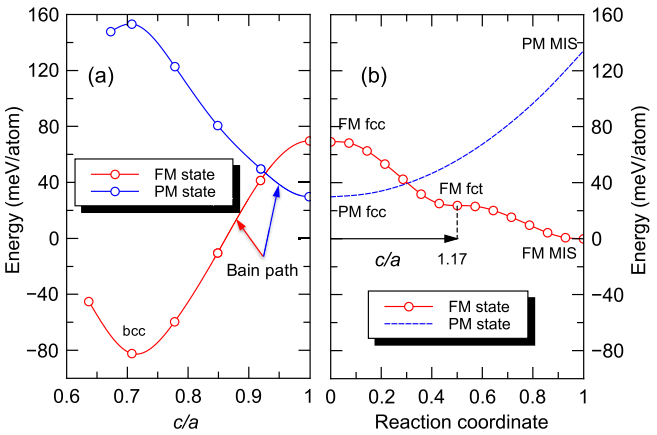

FIG. 4. (a) Energy variation of fcc Fe with respect to the c/a ratio in FM and PM states. (b) Minimum-energy path of the austenite → MIS transition in FM and PM states. The blue line in (a) is extracted from Ref. [54], which is based on the disordered local moment (DLM) method.

A. Austenite → MIS transition

The FM martensite is formed by quenching the high-temperature PM austenite. Hence, in this process, both structural and magnetic transitions occur. Since the MIS can either follow the PM state of austenite or adapt to the FM state of martensite, its magnetic state is not well defined. Hence, for the austenite → MIS transition, we consider two limiting cases in order to determine the magnetic state of the MIS: (i) PM austenite → PM MIS, (ii) FM austenite → FM MIS.

In the PM state, the PM MIS is unstable against atomic relaxations [see Fig. 4(b)]. Consequently, it directly relaxes to the PM austenite which is dynamically stable [55,56]. However, if we switch to the FM state, the FM austenite is unstable and transforms to the FM MIS with a two-step path as revealed by the SSNEB simulations. The first step is a tetragonal distortion to form face-centered-tetragonal (fct) Fe with a c/a ratio of 1.17. As shown in Fig. 4(a) for comparison, such tetragonal distortion proceeds opposite to the normal Bain path [13]. In the second step, only a minor atomic shuffle [see Fig. 2(c)] is required to transform the FM fct Fe to FM MIS.

The PM MIS is unstable and energetically so unfavorable that its energy is comparable with that of PM bcc Fe. It is thus unlikely that the PM state is still maintained in the MIS during quenching the PM austenite. Hence, we assume that during the formation of the MIS, the magnetic transition from PM to FM is already accomplished. In particular, as shown by Okatov *et al.* [57], a tetragonal distortion of austenite would induce a strong FM coupling and thus significantly increase the critical magnetic temperature of austenite up to ∼500 K. The coupling between the magnetic configuration and the lattice distortion assists the PM fcc → FM fct Fe transition. Our calculations show an energy barrier for the spin flips of ∼15 meV/atom at $T = 0$ K [see the intersection between blue and red lines in Fig. 4(b)], which agrees well with the estimated energy barrier reported by Okatov *et al.* [54] for the PM fcc → FM bcc Fe transition. In addition, temperature-induced vibrational and magnetic excitations also play an important role in the relative phase stability. However, as estimated in Ref. [8], this

will not change the qualitative picture of the PM austenite → FM MIS transition.

The above discussion does not yet include C interstitials. For the FM fct Fe → FM MIS transition, by placing one C interstitial on the OIS in the orthorhombic unit cell, as shown in Fig. 2, the picture remains qualitatively unchanged. Specifically, the FM fct Fe → FM MIS transition is still barrier free. Since only small atomic shifts of Fe atoms are involved in the transition, the C interstitial needs to adjust its atomic position only slightly. Moreover, the PM MIS including one C interstitial is still unstable against atomic relaxations and a direct relaxation to PM austenite is observed. Notably, the configurational entropy change induced by C redistribution also contributes to the relative phase stabilities of austenite and martensite. However, considering the maximum C content studied in this work, 8 at.% with an upper limit for the transition temperature of 1000 K, the free energy change due to configurational entropy is ∼8 meV/Fe atom, which might have a noticeable contribution, but does not change the qualitative picture of the transition pathways.

B. MIS → martensite transition

Since our calculations show that the C interstitial experiences only small displacements to keep in its local minimum during the PM austenite → FM MIS transition, the three scenarios for C redistribution indicated in Fig. 3 still exist for the MIS → martensite transition. In the following, we will systematically investigate the three scenarios as introduced in Sec. III.

Within each scenario of the C redistribution, there are three subscenarios corresponding to the cases of C redistribution onto three sublattices in martensite, respectively. For scenario S1 [see Fig. 5] where C preferentially occupies sublattice 1 (subscenario 1), next to the displacive rearrangement of the Fe lattice, the C atom performs only a minor displacement

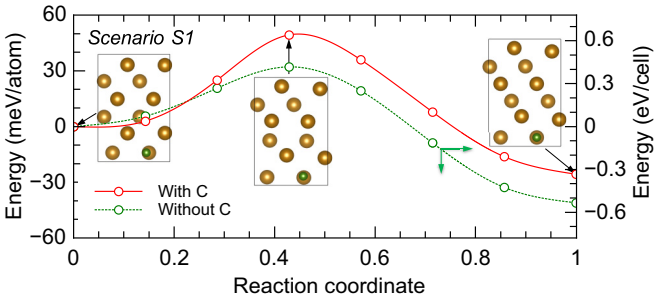

FIG. 5. Minimum-energy path of the MIS → martensite transition in scenario S1. The energy values in the red line are given in two different units by the left (total energy divided by total number of atoms) and right (total energy of the cell) y axes, respectively. To show the relative difference, the MEP of the case without C (green line) is vertically aligned to have the identical starting point with the one with C (red line). As indicated by the green arrows, the energy values in the green line refer to the right y axis. The structural evolution including the simultaneous motion of both Fe and C atoms is also shown in the figure. To maintain a continuity along the MEP, Fe atoms in different structures/phases are all represented by gold spheres, while the C interstitial is denoted by small green spheres.

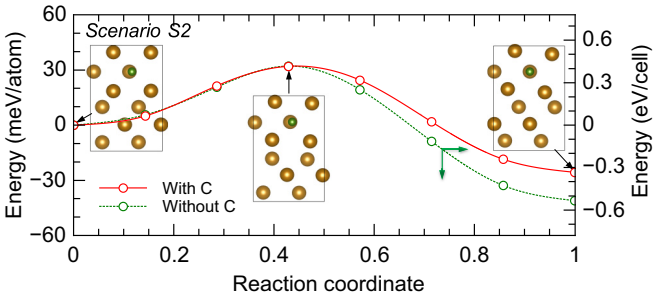

FIG. 6. Minimum-energy path and structural evolution of the MIS → martensite transition in scenario S2. The color code and energy definitions are the same as in Fig. 5.

(∼0.03 Å). The energy barrier for this case is 49 meV/atom with the present C concentration. If C is forced onto sublattices 2 or 3 (subscenarios 2 or 3), then a two-step process occurs. First, the system follows the same path as subscenario 1. Then a single atomic hop of the C atom between two adjacent OISs in martensite from sublattices 1 to 2 (or 3) is performed, which requires overcoming a C diffusion barrier of 0.86 eV. The value obtained from the NEB calculations agrees well with the experimental result of 0.87 eV [58] and the previous theoretical prediction of 0.86 eV [59]. However, for the diffusionless martensitic transformation, the transformation temperature is too low and the interface migration speed is too high for C to perform the atomic hop between OISs in martensite. Hence, for scenario S1, C interstitials would end up on sublattice 1 in martensite.

As shown in Fig. 6, scenario S2 is very similar to scenario S1. To be more specific, only a small displacement (∼0.38 Å) of the C atom is required if it is forced onto sublattice 1 (subscenario 1), and needs to overcome an energy barrier of 32 meV/atom with the present C concentration. If the C atom is forced onto sublattices 2 or 3 (subscenarios 2 or 3), then an additional atomic hop of C between OISs in martensite is again kinetically suppressed during the diffusionless martensitic transformation. Hence, in scenario S2, C interstitials will be preferentially transferred onto sublattice 1.

Scenario S3 qualitatively differs from scenarios S1 and S2. As shown in Fig. 7, the MEPs of the transformations involving C redistribution onto all three sublattices are nearly the same. The major difference between the three subscenarios lies in the

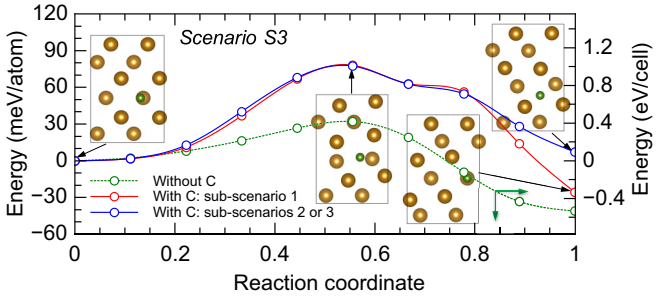

FIG. 7. Minimum-energy path and structural evolution of the MIS → martensite transition in scenario S3. The color code and energy definitions are the same as in Fig. 5.

energies of the final configurations of the martensite. This is because we have fixed the shape and the lattice constants of the simulation cell, which leads to the energy difference between the configurations with C on different sublattices in martensite. This is a technical limitation of the current approach. However, we will show later in Sec. VI that if we do not fix the cell shape, the shuffle-dominated transformation paths could not be directly simulated.

According to the visualized structural evolution in Fig. 7, the same barrier height in three subscenarios is not coincident, but is because they share the same mechanism. Specifically, the redistribution of C onto any sublattice in martensite is strongly influenced by a shearlike atomic shuffle of the Fe atoms. The motion of C is restricted by the initial OIS in the MIS. During the rearrangement of the Fe lattice, C is forced to move together with the Fe octahedra around it. As a consequence, the saddle points along the MEPs of the three subscenarios are identical. Topologically, it is thus a critical point on the potential-energy surface from which three downhill paths to the three sublattices exist. As a result, no additional atomic hop is required. Notably, as one can see from Fig. 7, the energies of configurations when going down from the saddle point show a small deviation from a continuously decreasing curve. This is because there is an equal preference of C redistribution onto the three sublattices. In the first NEB image after the saddle point, C is strongly attracted by the OISs of three sublattices equivalently. This type of saddle point is known as the bifurcation point on the potential-energy surface [60].

C. Interplay between C redistribution and the displacive rearrangement of Fe lattice

In the MEPs described in Sec. V B, the motions of Fe and C atoms are coupled. Thus, the energy barriers discussed so far are a superposition of two activated subprocesses: the MIS → bcc Fe transition and the transport of the C interstitial. In order to understand the interplay between these two subprocesses, we examine, on the one hand, the influence of the presence of a C interstitial on the MEP of the MIS → martensite transition.

Specifically, the MEPs of the MIS → martensite transition with a C interstitial shown in Figs. 5–7 are subtracted by the MEP of the case without C using a consistent unit of total energy per supercell. As shown in Fig. 8, for scenarios S1 and S2, only a small monotonous change in the energies along the transformation path is found. As a result, there is a slight increase (∼0.2 eV/C atom) in the total energy barrier in scenario S1, while there is almost no increase in the total energy barrier in scenario S2. This is understandable since for scenarios S1 and S2 the C interstitial displaces only slightly (<0.4 Å). The energy difference between the two endpoints (reaction coordinates equal to 0 and 1, respectively) is due to the different solution enthalpy of the C interstitial in the MIS and martensite.

For scenario S3, independent of which sublattice the C interstitial is transported onto, there is a remarkable enhancement of the total energy barrier (∼0.6 eV/C atom). Such an enhancement would significantly increase the difficulty of the martensitic phase transformation at the same temperature. To check if this increase in the energy barrier depends on C concentration, we perform NEB simulations of the MIS → martensite transition in scenario S3 with lower C concentrations by extending the supercell size and placing still one C atom in the supercell. The results shown in Fig. 9 reveal that the enhancement of the energy barrier due to the presence of C shows a significant reduction with decreasing C concentration. This is because the rearrangement of the Fe lattice to realize the transformation primarily involves a shearlike shuffle of two adjacent $(11\bar{2})$ Fe layers in the middle (along the *b* direction), as shown by the structural evolution in Figs. 5–7. The presence of the C interstitial acts as a local obstacle for the atomic shuffle of the Fe lattice and thus

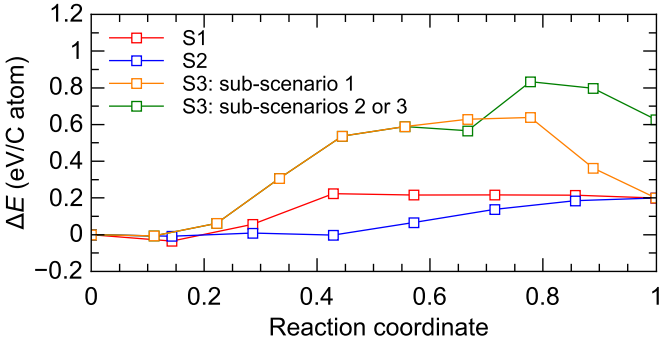

FIG. 8. The effect of the C interstitial on the minimum-energy path of the MIS → martensite transition in three different scenarios.

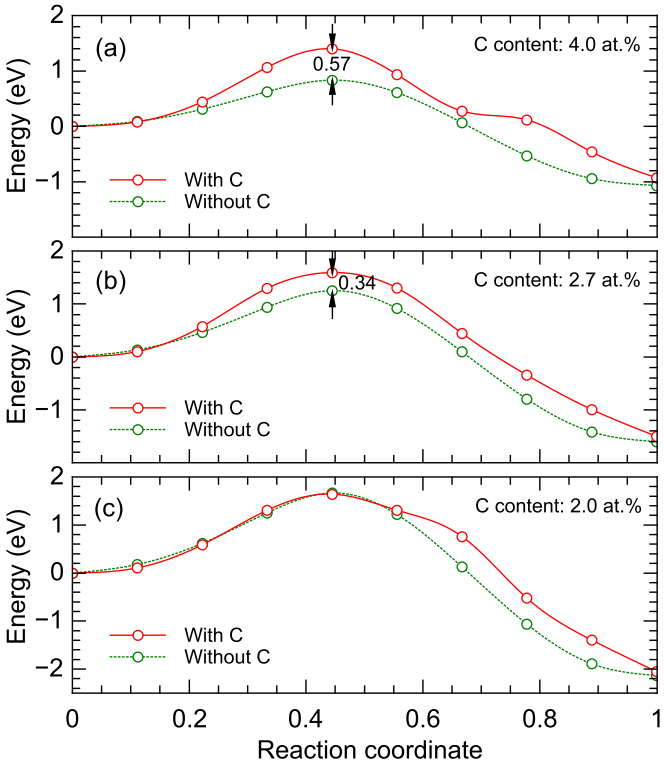

FIG. 9. Minimum-energy paths of the MIS → martensite transition in scenario 3 (subscenario 1) at various C concentrations: (a) 4.0 at.%; (b) 2.7 at.%; (c) 2.0 at.%. The minimum-energy paths in (a), (b), and (c) are computed by increasing the supercell size along the *a* axis by factors of 2, 3, and 4 relative to the unit cells [see Figs. 2 and 3], respectively.

enhances the energy barrier. A lower C concentration thus results in a smaller enhancement of the total energy barrier. More quantitatively, when the C content is reduced to below ~2 at.% [see Fig. 9(c)], the effect of C on the transformation barrier vanishes. Hence, for scenario S3, the C redistribution onto the octahedral sublattices in martensite is only possible if the C concentration is not too high. Once the C concentration exceeds a critical value, the energy barrier becomes too high to overcome during the martensitic transformation. Thus, for high concentrations, C would be trapped in the OISs of the MIS, which might then result in the formation of orthorhombic martensite [25] due to the anisotropic lattice distortion. Therefore, it can be concluded that the influence of the C interstitials on the displacive rearrangement of the Fe lattice is very localized. This influence becomes pronounced only when the C concentration reaches a certain level.

On the other hand, considering the impact of the MIS → martensite transition on the redistribution of the C interstitial, it is clear from Fig. 8 that in all three scenarios, the presence of C reduces the driving force of the phase transformation. The phase transformation is primarily driven by the energy reduction of the Fe lattice. C is basically forced to move in order to adjust itself to fit the transformation of the Fe lattice. In the configurations between the saddle point and martensite, C shows a relatively high solution enthalpy in scenario 3, as shown in Fig. 8. This part is, however, compensated by the drastic energy reduction of the Fe lattice and thus does not affect the total energy barrier of the phase transformation.

D. Origin of the abnormal interstitial redistribution

Based on the detailed analysis of the MEPs in the three scenarios of C redistribution, we are now able to compute the ratio of C interstitials that will be redistributed onto sublattice 1, which allows us to address the origin of the abnormal interstitial redistribution.

Combining the above results, we find that in contrast to the original concepts, C is not always redistributed onto a single sublattice in martensite. Since in the fcc matrix all C interstitial sites are equivalent, all three scenarios occur with equal probability. Furthermore, since sublattices 2 and 3 are identical due to symmetry, the ratio of C interstitials that will be transported onto sublattice 1 can thus be calculated as $1/3 + 1/3 + 1/3 \times 1/3 = 7/9 \simeq 78\%$.

Specifically, for scenarios S1 and S2, all C interstitials end up on sublattice 1, which yields $1/3 + 1/3$. As for scenario S3, when the C content is not too high, only $1/3$ of such C atoms will finally occupy sublattice 1, which can then be counted as $1/3 \times 1/3$. This predicted value of 78% agrees well with the experimentally measured result of about 80%. Notably, the experimental data of 80% was obtained from steels containing alloying elements. However, as shown by Al-Zoubi *et al.* [37], Mn and Cr have a negligible effect on the tetragonality of the martensite, and 5 at.% Ni could enhance the tetragonality by only 0.7%, which is also relatively small compared to the effect from fcc → bct structural transformation. Nevertheless, the close agreement cannot be regarded as a direct proof of the proposed transformation mechanism, but provides an intuitive explanation of the observed C distribution in the freshly formed martensite, which was missing in traditional transformation mechanisms such as the Bain path.

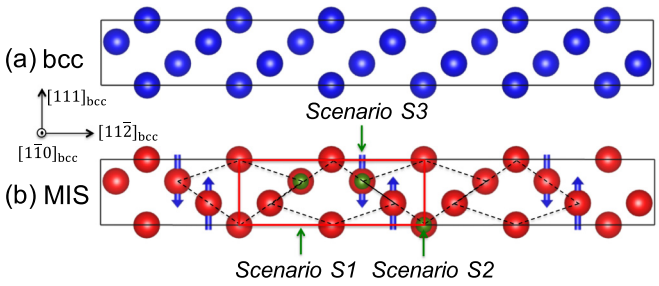

FIG. 10. Relation between the three scenarios for the C redistribution and the structural feature of the MIS. The black dashed lines show the bcc Σ3 twins in the MIS. Blue arrows indicate the Fe atoms that are strongly involved in the atomic shuffle to realize the MIS → martensite transition and the corresponding shuffling directions. Small green spheres represent the C interstitials. The red rectangle highlights one primitive cell of the MIS.

E. Atomistic origin of the three scenarios

In the previous sections, we found that the abnormal redistribution of interstitials is due to the existence of three different scenarios. However, it is still structurally unclear why there exist three different scenarios. In this section, we will address this question.

As shown by the black dashed lines in Fig. 10(b), the MIS consists of a periodic arrangement of Σ3 twin boundaries in bcc Fe. One can also see from Fig. 10 that the MIS → bcc Fe transition mostly involves a shearlike shuffle of two adjacent atomic layers along the $\pm[111]_{bcc}$ directions (the blue arrows). The shuffle is related to the well-known [111] slip directions in bcc metals. As shown in Fig. 10(b), the three scenarios correspond to structurally inequivalent locations of the interstitial sites in the MIS. For scenarios S1 and S2, the C atom is in the planes that do not shuffle during the transition. However, in scenario S3, C is located in the slip planes and is thus dragged by the moving Fe atoms to a saddle point from which C can go onto any of the three sublattices without having to overcome a barrier. This is the atomistic origin for the existence of three scenarios and for the distinction of scenario S3 from scenarios S1 and S2.

VI. MARTENSITIC TRANSFORMATION MECHANISM

In this section, we will briefly analyze the underlying mechanism of the martensitic transformation in terms of shear and atomic shuffle in order to understand the distinction of the present path from the conventional ones.

As shown by the green dashed box in Fig. 3(b), a rhomboidal unit cell can also be constructed based on the same OR [40]. Such a lattice correspondence shares a similar mechanism to the Bain, KS, or NW paths, as given in Fig. 1. Specifically, these paths only require a homogenous shear deformation of the cell and no internal atomic shuffles are required. This explains why for these transformation paths the sublattice ordering is 100%, i.e., all C atoms go onto the same sublattice in martensite. As shown by the blue line in

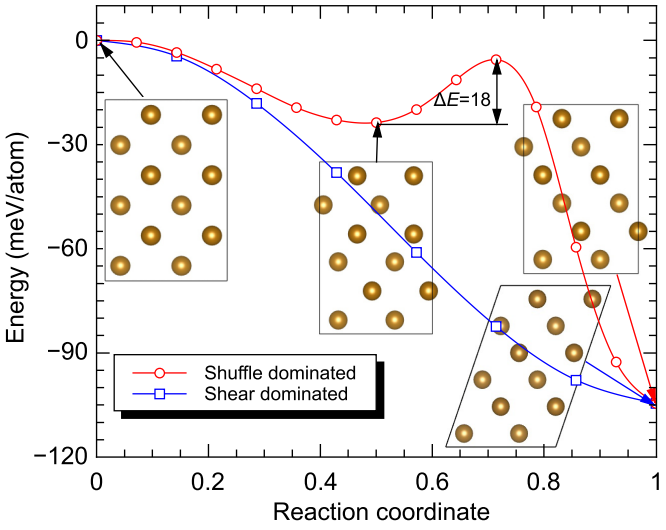

FIG. 11. Minimum-energy paths calculated by solid-state nudged elastic band simulations of the austenite (fct Fe) → martensite transition without a C atom in the ferromagnetic state. The red line stands for the shuffle-dominated mechanism, while the blue line stands for a shear-dominated one.

Fig. 11, the MEP based on this lattice correspondence between austenite and martensite is barrier free at $T = 0$ K. This is also true for the normal Bain, KS, or NW paths [61]. However, it needs to be noted that such transformation paths would induce a large elastic strain (e.g., principal strains of Bain path: +12%, +12%, and −20% [62]) of the material. Therefore, although there is no energy barrier at $T = 0$ K for the atomic rearrangement, it produces large elastic mismatch energies (of the order of 0.1 eV per interface atom as estimated by linear elasticity theory [63]) at the austenite/martensite interface.

Instead, our proposed path for the martensitic transformation realizes the cell distortion and volume expansion by a tetragonal distortion of fcc Fe (see lattice parameters as provided in Table I). Afterwards, the fct Fe → MIS → martensite transition mostly involves atomic shuffles with minor changes in the lattice constants and cell shape. As derived by Cayron [62], the principal strains of the Pitsch OR used in this work are well below those of the Bain, KS, or NW ORs. Although there is an energy barrier of 18 meV/atom for the MIS → martensite transition, the elastic energy induced by the phase transition would be much smaller than that in other paths. Hence, considering the total energy cost, the present path is still more favorable. More importantly, only within this shuffle-dominated mechanism, the three different C redistribution scenarios and thus the abnormal C redistribution are possible, which is a key feature of the martensitic transformation in Fe-C alloys. We do not find a shuffle-dominated lattice correspondence based on the Bain, KS, or NW ORs. However, if this can be done, the existence of different C redistribution scenarios due to the atomic shuffle is also expected.

VII. CONCLUSIONS

The martensitic transformation in Fe-C alloys distinguishes itself from many other martensitic transformations by combining a redistribution of C interstitials with a fcc → bcc structural transformation of the Fe lattice. A detailed study of the interplay between two subprocesses was required, since the abnormally low tetragonality of the freshly formed martensite observed in experiments cannot be explained by the conventional mechanisms.

In this paper, we therefore extend our recently proposed transition path for the fcc → bcc Fe transformation in order to include C interstitials. Performing NEB simulations to map the energetics of the various paths, we find that in contrast to the conventional transformation paths such as the Bain path, C ordering on the octahedral sublattices is no longer perfect. Due to the transformation, the originally equivalent interstitial sites for C atoms become crystallographically inequivalent: For 2/3 of the sites a transformation path to one of the sublattices is geometrically and energetically preferred, while for 1/3 of the sites a symmetry break occurs that allows the C atom to occupy with equal probability any of the three inequivalent interstitial sublattices in martensite. This finding naturally explains why in contrast to thermodynamic considerations only ∼80% of the C atoms go onto the thermodynamically preferred sublattice sites and addresses the abnormally low tetragonality of the freshly formed martensite.

The microscopic origin is the drag of C atoms caused by the shearlike shuffle of adjacent $(11\bar{2})$ Fe layers along the $\pm[111]_{bcc}$ directions during the displacive rearrangement of the Fe lattice. The combination of shear (the tetragonal distortion of fcc Fe) and atomic shuffle in a single displacive mechanism clearly differs from homogenous deformation paths such as the Bain path. The combined occurrence of these two mechanisms naturally results in the occupation of C on all three octahedral sublattices in martensite. We expect that the methodological approach employed here to describe the interplay between interstitial displacement and martensitic transformations is general and also applicable for modeling the motion of other interstitial elements during displacive rearrangements of the host material.

ACKNOWLEDGMENTS

We gratefully acknowledge the financial support of the Max-Planck Society within the International Max Planck Research School for Surface and Interface Engineering in Advanced Materials (IMPRS-SurMat) at the Max-Planck-Institut für Eisenforschung GmbH and of the Deutsche Forschungsgemeinschaft within the collaborative research center SFB761 “Stahl - *ab initio*.” Our sincere gratitude also goes to F. Körmann and B. Dutta for fruitful discussions and kind assistance.

[1] S. Fabris, A. T. Paxton, and M. W. Finnis, Phys. Rev. B **63**, 094101 (2001).

[2] M. A. Uijttewaal, T. Hickel, J. Neugebauer, M. E. Gruner, and P. Entel, Phys. Rev. Lett. **102**, 035702 (2009).

[3] B. Dutta, A. Çakır, C. Giacobbe, A. Al-Zubi, T. Hickel, M. Acet, and J. Neugebauer, Phys. Rev. Lett. **116**, 025503 (2016).
[4] S. A. Nikitin, K. P. Skokov, Yu. S. Koshkid'ko, Yu. G. Pastushenkov, and T. I. Ivanova, Phys. Rev. Lett. **105**, 137205 (2010).
[5] M. Ye, A. Kimura, Y. Miura, M. Shirai, Y. T. Cui, K. Shimada, H. Namatame, M. Taniguchi, S. Ueda, K. Kobayashi, R. Kainuma, T. Shishido, K. Fukushima, and T. Kanomata, Phys. Rev. Lett. **104**, 176401 (2010).
[6] A. Martens, Z. Ver. Deut. Ing. **22**, 11 (1878).
[7] R. G. Hennig, D. R. Trinkle, J. Bouchet, S. G. Srinivasan, R. C. Albers, and J. W. Wilkins, Nat. Mater. **4**, 129 (2005).
[8] X. Zhang, T. Hickel, J. Rogal, S. Fähler, R. Drautz, and J. Neugebauer, Acta Mater. **99**, 281 (2015).
[9] W. L. Fink and E. D. Campbell, Trans. Am. Soc. Steel Treat. **9**, 717 (1926).
[10] N. Seljakov, G. Kurdjumov, and N. Goudsov, Z. Phys. **45**, 384 (1927).
[11] G. V. Kurdjumov and E. Kaminsky, Nature (London) **122**, 475 (1928).
[12] G. V. Kurdjumov and E. Kaminsky, Z. Phys. **53**, 696 (1929).
[13] E. C. Bain, Trans. AIME **70**, 25 (1924).
[14] G. V. Kurdjumov and G. Sachs, Z. Phys. **64**, 325 (1930).
[15] Z. Nishiyama, Sci. Rep. Res. Inst. Tohoku Univ. **23**, 638 (1934).
[16] G. Wassermann, Arch. Eisenhüttenwes. **6**, 347 (1933).
[17] L. I. Lyssak and Ja. N. Vovk, Fiz. Met. Metalloved. **20**, 540 (1965).
[18] L. I. Lyssak, Ja. N. Vovk, and Ju. M. Polishchuk, Fiz. Met. Metalloved. **23**, 898 (1967).
[19] L. I. Lyssak and L. O. Andrushchik, Fiz. Met. Metalloved. **28**, 348 (1969).
[20] L. I. Lyssak and Ja. N. Vovk, Fiz. Met. Metalloved. **31**, 646 (1971).
[21] I. R. Entin, V. A. Somenkov, and S. Sh. Shilstein, Dokl. Akad. Nauk USSR **206**, 1096 (1972).
[22] S. Allain, F. Danoix, M. Goune, K. Hoummada, and D. Mangelinck, Philos. Mag. Lett. **93**, 68 (2012).
[23] L. I. Lyssak, S. A. Artimiuk, and Ju. M. Polishchuk, Fiz. Met. Metalloved. **35**, 1098 (1973).
[24] M. Watanabe and C. M. Wayman, Scr. Metall. **5**, 109 (1972).
[25] L. I. Lyssak, S. P. Kondratiev, and Ju. M. Polishchuk, Fiz. Met. Metalloved. **36**, 546 (1973).
[26] L. I. Lyssak and B. I. Nikolin, Fiz. Met. Metalloved. **22**, 730 (1966).
[27] A. L. Roytbourd and A. G. Khachaturyan, Fiz. Met. Metalloved. **30**, 1189 (1970).
[28] G. V. Kurdjumov and A. G. Khachaturyan, Acta Metall. **23**, 1077 (1975).
[29] G. V. Kurdjumov, Metall. Trans. A **7**, 999 (1976).
[30] G. V. Kurdjumov and A. G. Khachaturyan, Metall. Trans. **3**, 1069 (1977).
[31] S. Kajiwara and T. Kikuchi, Acta Metall. Mater. **39**, 1123 (1991).
[32] J. W. Christian, Mater. Trans., JIM **33**, 208 (1992).
[33] M. Oka and C. M. Wayman, Trans. Am. Inst. Min. Engrs. **242**, 337 (1968).
[34] M. Watanabe and C. M. Wayman, Metall. Trans. **2**, 2221 (1971).
[35] F. E. Fujita, Metall. Trans. A **8**, 1727 (1977).
[36] S. Uehara, S. Kajiwara, and T. Kikuchi, Mater. Trans., JIM **33**, 220 (1992).
[37] N. Al-Zoubi, N. V. Skorodumova, A. Medvedeva, J. Andersson, G. Nilson, B. Johansson, and L. Vitos, Phys. Rev. B **85**, 014112 (2012).
[38] S. J. Dillon, M. Tang, W. C. Carter, and M. P. Harmer, Acta Mater. **55**, 6208 (2007).
[39] K. Momma and F. Izumi, J. Appl. Crystallogr. **44**, 1272 (2011).
[40] W. Pitsch, Philos. Mag. **4**, 577 (1959).
[41] D. Sheppard, P. Xiao, W. Chemelewski, D. D. Johnson, and G. Henkelman, J. Chem. Phys. **136**, 074103 (2012).
[42] G. Henkelman and H. Jónsson, J. Chem. Phys. **113**, 9978 (2000).
[43] D. Sheppard, R. Terrell, and G. Henkelman, J. Chem. Phys. **128**, 134106 (2008).
[44] P. E. Blöchl, Phys. Rev. B **50**, 17953 (1994).
[45] J. P. Perdew, K. Burke, and M. Ernzerhof, Phys. Rev. Lett. **77**, 3865 (1996).
[46] G. Kresse and J. Furthmüller, Phys. Rev. B **54**, 11169 (1996).
[47] H. J. Monkhorst and J. D. Pack, Phys. Rev. B **13**, 5188 (1976).
[48] M. Methfessel and A. T. Paxton, Phys. Rev. B **40**, 3616 (1989).
[49] C. S. Roberts, Trans. AIME **197**, 203 (1953).
[50] N. I. Medvedeva, D. Van Aken, and J. E. Medvedeva, J. Phys.: Condens. Matter **22**, 316002 (2010).
[51] J. A. C. Bland, C. Daboo, B. Heinrich, Z. Celinski, and R. D. Bateson, Phys. Rev. B **51**, 258 (1995).
[52] A. van de Walle and G. Ceder, J. Phase Equilib. **23**, 348 (2002).
[53] See Supplemental Material at http://link.aps.org/supplemental/10.1103/PhysRevB.94.104109 for all of the structural details (animations and original structure files, etc.) of the simulated transformation pathways in this work.
[54] S. V. Okatov, A. R. Kuznetsov, Y. N. Gornostyrev, V. N. Urtsev, and M. I. Katsnelson, Phys. Rev. B **79**, 094111 (2009).
[55] F. Körmann, A. Dick, B. Grabowski, T. Hickel, and J. Neugebauer, Phys. Rev. B **85**, 125104 (2012).
[56] F. Körmann, T. Hickel, and J. Neugebauer, Curr. Opin. Solid State Mater. Sci. **20**, 77 (2016).
[57] S. V. Okatov, Y. N. Gornostyrev, A. I. Lichtenstein, and M. I. Katsnelson, Phys. Rev. B **84**, 214422 (2011).
[58] C. Wert and C. Zener, Phys. Rev. **76**, 1169 (1949).
[59] D. E. Jiang and E. A. Carter, Phys. Rev. B **67**, 214103 (2003).
[60] D. Sheppard and G. Henkelman, J. Comput. Chem. **32**, 1769 (2011).
[61] I. K. Razumov, D. V. Boukhvalov, M. V. Petrik, V. N. Urtsev, A. V. Shmakov, M. I. Katsnelson, and Y. N. Gornostyrev, Phys. Rev. B **90**, 094101 (2014).
[62] C. Cayron, Acta Crystallogr. Sect. A **69**, 498 (2013).
[63] A. Biedermann, M. Schmid, and P. Varga, Phys. Rev. Lett. **86**, 464 (2001).